frontiers | Frontiers in Earth Science

TYPE Original Research
PUBLISHED 13 August 2024
DOI 10.3389/feart.2024.1437605

OPEN ACCESS

EDITED BY
Olusola Oluwayemisi Ololade,
University of the Free State, South Africa

REVIEWED BY
Ameha Atnafu Muluneh,
Addis Ababa University, Ethiopia
Bisrat Yibas,
University of the Free State, South Africa

*CORRESPONDENCE
Fan Zheng,
zhengfan@aircas.ac.cn

RECEIVED 24 May 2024
ACCEPTED 31 July 2024
PUBLISHED 13 August 2024

CITATION
Zheng F, Xu T, Ai Y, Ge Y, Zeng Q, Miao L, Dong W and Badal J (2024) Deep structure of the Wulong goldfield, Liaodong Peninsula, China, revealed by receiver functions: implications for the tectonic and mineralization dynamics.
Front. Earth Sci. 12:1437605.
doi: 10.3389/feart.2024.1437605

Deep structure of the Wulong goldfield, Liaodong Peninsula, China, revealed by receiver functions: implications for the tectonic and mineralization dynamics

Fan Zheng[1,2,3]*, Tao Xu[4,5], Yinshuang Ai[5,6,7], Yunping Ge[1,2,3], Qingdong Zeng[4,5,7], Laicheng Miao[4,5], Weiyu Dong[1,2,3] and José Badal[8]

[1]Aerospace Information Research Institute, Chinese Academy of Sciences, Beijing, China, [2]Key Laboratory of Target Cognition and Application Technology (TCAT), Aerospace Information Research Institute, Chinese Academy of Sciences, Beijing, China, [3]Key Laboratory of Network Information System Technology (NIST), Aerospace Information Research Institute, Chinese Academy of Sciences, Beijing, China, [4]Key Laboratory of Mineral Resources, Institute of Geology and Geophysics, Chinese Academy of Sciences, Beijing, China, [5]Innovation Academy for Earth Science, Chinese Academy of Sciences, Beijing, China, [6]Key Laboratory of Earth and Planetary Physics, Institute of Geology and Geophysics, Chinese Academy of Sciences, Beijing, China, [7]College of Earth and Planetary Sciences, University of Chinese Academy of Sciences, Beijing, China, [8]Physics of the Earth, University of Zaragoza, Zaragoza, Spain

During the Mesozoic, the North China Craton experienced intense tectonic movements that resulted in the formation of numerous gold deposits on the Liaodong and Jiaodong Peninsulas in northeastern China. To investigate the relationship between deep crustal structure and gold mineralization in the Liaodong Peninsula, we deployed 334 dense seismic stations in the Wulong goldfield (WLGF) with the idea of analysing numerous receiver functions at different array stations. The purpose focused on knowing the potential for gold mineralization in the area. The study revealed the following: (1) The WLGF is characterized by a crustal thickness of approximately 32 km and an average Vp/Vs ratio of 1.76. The high value of the Vp/Vs ratio near the Wulong gold deposit suggests that mantle materials have penetrated into the crust and contributed to the mineralization process. (2) A low-velocity layer located at a depth of 10–18 km below the WLGF seems to support the existence of a potentially brittle-ductile transition zone. Also, hydrothermal magma upwelling channels are observed in the upper crust beneath the Wulong gold deposit. (3) The presence of a discontinuous low-velocity layer in the middle crust beneath the Liaodong Peninsula suggests promising prospects for gold ore exploration. The receiver functions method based on a dense seismic array employed in this study can offer valuable references and guidance for the fine exploration and research of ore deposits in other regions globally.

KEYWORDS

dense seismic array, receiver functions, crustal imaging, metallogenic potential, Wulong goldfield (Liaodong Peninsula)

1 Introduction

The word craton means a stable geological unit on the continental crust (Santosh et al., 2007). However, intense metamorphic tectonic movements occurred in the eastern part of the North China Craton (NCC) during the Mesozoic period, driven by the ongoing westward subduction of the Western Pacific Plate, resulted in a thinning of the lithosphere thickness that was accompanied by intense gold mineralization (Zhu et al., 2015; Meng et al., 2021). Thus, the eastern NCC became home to numerous and important gold deposits, including the Linglong gold deposit in Shandong Province and the Wulong goldfield (hereinafter WLGF) in Liaoning Province (Wei et al., 2001 Wei et al., 2004; Song, 2015). The Jiaodong Peninsula has confirmed ore reserves of more than 5,000 tons, making it the world's third-largest gold deposit cluster (Deng et al., 2020). In contrast, the Liaodong Peninsula currently only has reserves of about 500 tons, much less than Jiaodong (Zeng et al., 2019). However, the same tectonic framework and metallogenic epoch affect both peninsulas lead to speculation that there may be additional gold reserves in deeper structures of the Liaodong Peninsula (Di et al., 2021). The spatial distribution of these confirmed gold reserves does not follow any particular pattern and is extremely uneven.

In view of the aforementioned dissimilarity, numerous previous studies have focused on comprehensive investigations into the deep structure of the Liaodong Peninsula (Zheng et al., 2015; Xie et al., 2021; Dong et al., 2022; Ma et al., 2022; Zheng et al., 2022). Zheng et al. (2015) used receiver functions to obtain the seismic velocity structure in northeast China and shed light on the crustal evolution in this region caused by magmatic and metamorphic tectonic processes in an extensional context. Dong et al. (2022) used a dense seismic array and the same method to determine the deep tectonic boundary between the NCC and the Central Asian Orogenic Belt. Ma et al. (2022) obtained a clearer seismic velocity structure of the lithosphere beneath the Liaodong Peninsula. The results provided by these studies mainly focus on the large-scale structure of the Liaodong Peninsula; but in recent years the fine structure associated with each of the gold deposits in this area has also been the subject of attention. For example, Xie et al. (2021) revealed the influence of deep intrusive rocks on gold mineralization in the Qingchengzi goldfield of the Liaodong Peninsula and proposed a geologically reasonable model related to deep potential deposits. Zheng et al. (2022) used high-resolution ambient seismic noise tomography to discover a hidden NW-trending fault in the shallow part of the WLGF in Liaodong, which may be an important channel for fluid migration, and identified three potential areas of mineralization. It has been speculated that there may be other areas of fluid activity in the northwest zone of the gold deposit, with buried intrusive rocks that constitute the source of mineralization (Zeng et al., 2019).

The extensive research conducted on the Liaodong Peninsula and its adjacent areas has predominantly faced two key challenges: (1) previous studies are generally based on wide-bandwidth data with limited resolution and do not meet the requirements for a precise mineral exploration; (2) studies carried out on gold deposits reach relatively shallow depths (<3 km), which does not clarify the dynamics of ore formation at greater depth. To address these issues, in this paper we perform an in-depth analysis of receiver functions based on an extensive seismic data set collected by the Wulong dense short-period (WSP) array deployed on the Liaodong Peninsula. Taking advantage of seismic evidence, we explore deep mineralization processes in the Liaodong Peninsula as a guide for prospecting tasks in the mining area.

In this study, we employed a receiver function method based on a dense seismic array. By stacking teleseismic receiver functions from adjacent stations, we enhanced both the accuracy and continuity of the receiver functions while preserving the high precision of the array, resulting in high-resolution crustal structure in the goldfield. This method is applicable to fine exploration of ore deposits in other regions (e.g., Liu et al., 2018; Wei et al., 2018; Yu et al., 2020c; Jiang et al., 2020; Lythgoe et al., 2020; Zhang et al., 2020; Zhang et al., 2021), with particular effectiveness in identifying migration pathways of ore-bearing fluids. This aids in understanding the structural characteristics at different depths within mineralization zones and their impact on mineralization, providing strong support for targeted gold exploration.

2 Geological setting

The WLGF is located northeast of the NCC (Figure 1). There are a large number of Mesozoic granitic intrusions spread throughout the area that mainly make up the Wulongbei, Wulong and Sanguliu plutons (Wu et al., 2005). The Wulong pluton is mainly composed of hornblende granite and biotite granite intruded during the Late Jurassic ~160 Ma ago, which are widely distributed throughout the area (Wu et al., 2005). The Sanguliu pluton contains two rock types: its edge is composed of diorite (and minor quartz diorite), while its centre is composed of granodiorite. Zircon dating demonstrates that the intrusion of these two rock types occurred approximately 131–120 Ma ago (Wang et al., 2020). The Wulongbei pluton is composed of diorite with a spot structure and was formed during the Early Cretaceous, with a U-Pb zircon age of ~127 Ma (Yu et al., 2020a).

Two sets of faults with NE- and NW-trendings cross the Wulong pluton (Figure 1) (Zheng et al., 2022). The NE-trending Yalu River fault (east of the study area), is a first-order fault that has influenced the development of a series of NE-trending sinistral strike-slip faults (Hanjiapu, Hongshi, Yangjia, Jixingou, 100#, Heigou and Zhengjiapuzi) with strike of 25°–30°, NW dip direction and a dip angle of 50°–80° (Yu et al., 2020b). In addition, there are also some NW-trending hidden faults (NWF1 and NWF2) in the Wulong area, which partially outcrop to the east of this goldfield (Figure 1). These NW-trending faults have a strike of about 320°, dip towards the SW with angles between 50° and 70°, and traverse the entire goldfield. Both NW- and NE-trending faults in the WLGF are conjugate faults and constitute the main fault system governing the localization of gold deposits (Zheng et al., 2022).

3 Data and methods

3.1 Seismic data

This study is based on seismic data recorded by the WSP array deployed in Dandong, Liaoning, in May 2019. The size of this seismic array covered an area of 27 km^2 × 7 km^2 (Figure 2). The average

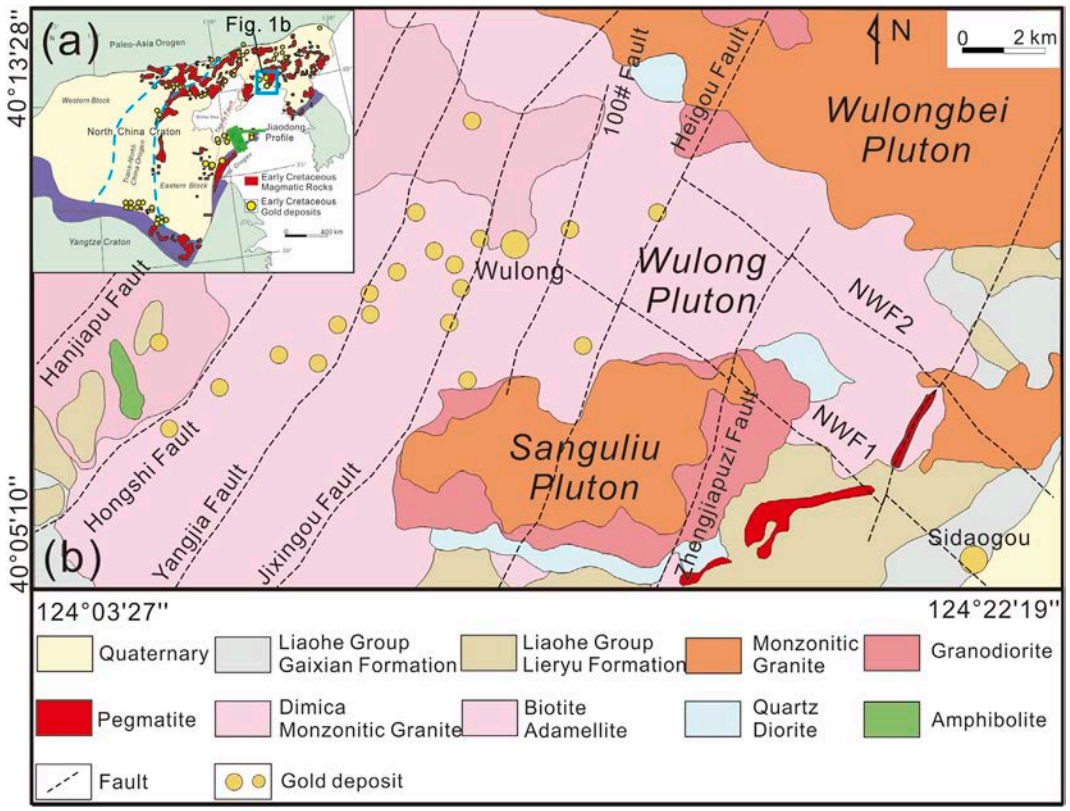

FIGURE 1
(A) Early Cretaceous gold deposits (yellow circles) and magmatic rocks (in red) in the North China Craton (Zhu et al., 2015). The small blue rectangle in the upper left inset delimits the study area; the green line "Jiaodong Profile" marks the location of the profile in Figure 8 (Yu et al., 2020c). **(B)** The geological structure map of Wulong in Liaodong (Gu et al., 2020). Yellow circles show locations of gold deposits. Dashed lines indicate local faults trending approximately N-S; in particular, NWF1 and NWF2 are NW-trending faults.

distance between adjacent stations ranged from 0.5 to 1 km. The array included 334 short-period seismometers and was in operation for 1 month. In anticipation of data with low signal-to-noise ratio, we only considered teleseismic events with magnitude above 5.5 as data sources.

From the available information provided by the earthquake catalogue edited by the United States Geological Survey (USGS), we gathered 26 earthquakes that meet the requirements (teleseisms with M > 5.5) of this study. All of these events are shown as red circles on Figure 3.

All collected data were pre-processed according to the following operations: (a) resampling of the raw data from 250 to 25 Hz to improve computational efficiency; (b) rotation of the Z-N-E components to the Z-R-T components; (c) bandpass filtering (0.01–1 Hz) to preserve the information supplied by body waves; (d) removing of instrument response to improve the signal-to-noise ratio; (e) zero-line slope detrending and tapering to improve the stability of subsequent data processing.

3.2 P-wave receiver function extraction

We used iterative deconvolution in the time domain (Ligorría and Ammon, 1999) to extract P-wave receiver functions. With the idea of more clearly identifying crustal seismic phases, we filtered the receiver functions with a Gaussian filter of coefficient 5.0. Finally, we obtained 1,513 high-quality receiver functions.

The lack of quality of single-station receiver functions prompted us to adopt a linear stacking approach to combine the receiver functions of adjacent stations within a distance range of 1.5 km. This method is effective in suppressing interfering signals and thus improving the signal-to-noise ratio. Figure 4 includes a comparison of receiver functions obtained at stations WL303 and WL924 before and after stacking.

3.3 H-κ stacking

To determine the depth of the Moho discontinuity, we used the H-κ stacking method (Zhu and Kanamori, 2000) to maximize the stacking amplitude of the $s(H,\kappa)$ function and find the optimal values of H and κ:

$$s(H,\kappa) = \omega_1 r(t_{Ps}) + \omega_2 r(t_{PpPs}) - \omega_3 r(t_{PpPs+PsPs}), \quad (1)$$

where ω_1, ω_2 and ω_3 are the weights given to the Ps, PpPs and PpSs+PsPs phases, respectively. H represents the depth of the Moho discontinuity and κ is the Vp/Vs ratio. For data processing we assigned weights of 0.5 to the Ps phase, 0.3 to the PpPs phase, and

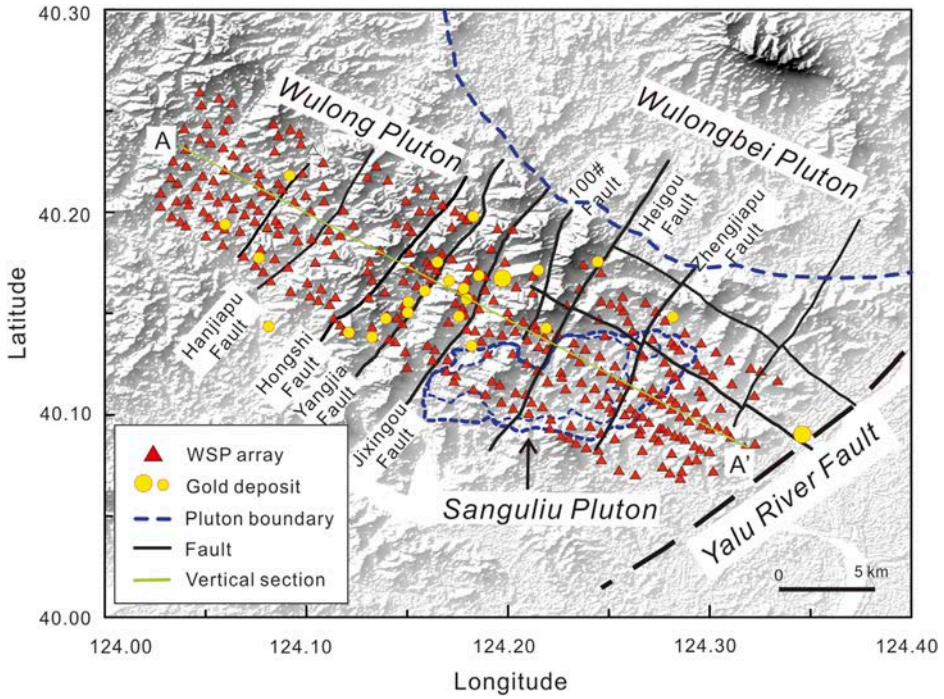

FIGURE 2
Wulong goldfield short-period (WSP) seismic array in the Liaodong Peninsula, northeast China. The red triangles represent seismic stations deployed in the study area. Yellow circles show locations of gold deposits. The green line A-A′ in the NW-SE direction marks the location of the vertical cross-section discussed later (Zheng et al., 2022). Faults as in Figure 1. The dashed blue line is the boundary between the Wulongbei Pluton (northeast quadrant) and the Sanguliu Pluton (outlined by a closed dashed blue line in the middle of the chart).

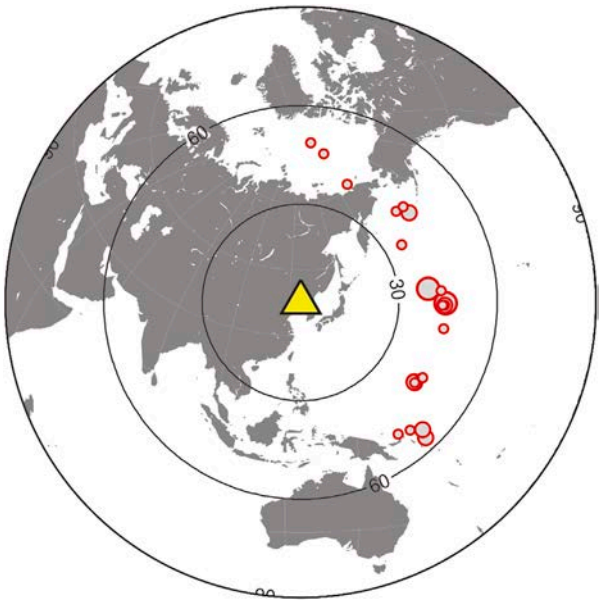

FIGURE 3
Geographical location of the teleseismic events: red circles drawn on a world map represent earthquake epicenters. The yellow triangle in the centre of the illustration marks the location of the WSP array (see Figure 2).

0.2 to the PpSs+PsPs phase, and scanned the crustal depth range H from 25 to 40 km and the variation range of κ from 1.5 to 1.9 for each short-period recording station. As an example, Figure 5 shows the H-κ scanning results for each of the aforementioned phases and also the weighted stacking result for station WL105. Subsequently, after applying the method to all stations of the two-dimensional array, we gathered all the H-κ scanning results to obtain a map of the Moho depth and Vp/Vs ratio in the WLGF, including their associated uncertainties, as shown in Figure 6.

3.4 CCP stacking imaging

To image the seismic velocity structure of the crust beneath the WLGF, we used a common conversion point (CCP) stacking which involves projecting the amplitudes of all phases of the receiver functions onto the P-to-S conversion point determined by the time delay with respect to the direct P wave (Zhu and Kanamori, 2000). To do this, we took the IASP91 global standard model as a reference and used a grid with CCP stacking dimensions of 0.1 km (profile), 1 km (horizontal), and 0.5 km (depth).

The earthquakes selected for our analysis are distributed to the east or southeast of the WSP array (Figure 3), so that the incidence point of the seismic ray is roughly located beneath the array. The implementation of the CCP stacking method allowed us to successfully generate a comprehensive image of the crustal

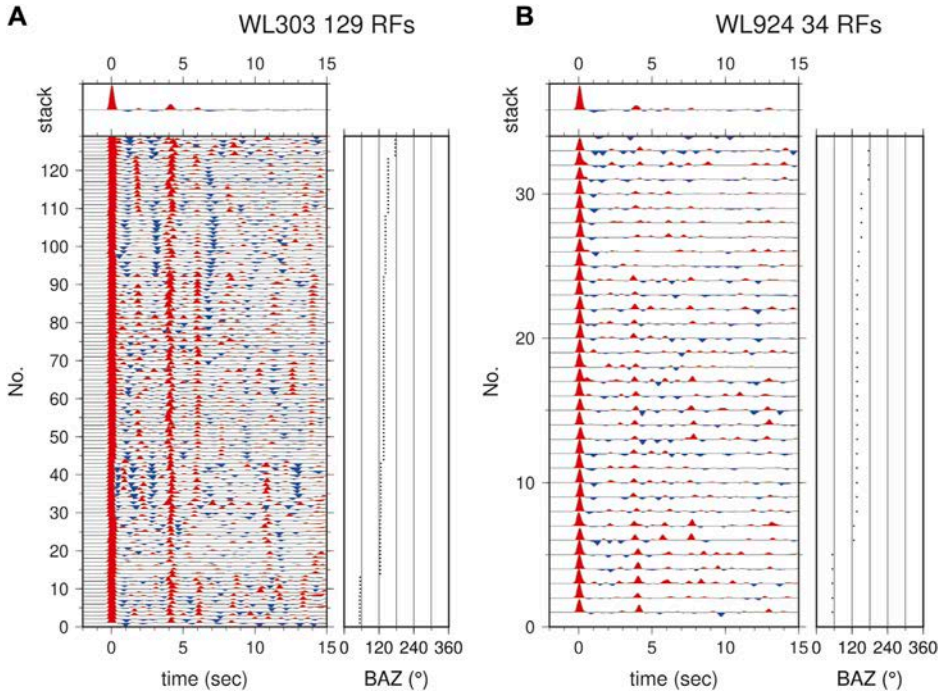

FIGURE 4
Comparison of receiver functions obtained at stations WL303 **(A)** and WL924 **(B)** before and after stacking. In this illustration, the panels on the left show the individual receiver functions before stacking, while the top panels show the receiver function after stacking. The panels on the right display the back-azimuth corresponding to each receiver function. The first example shows 129 receiver functions, while the second only 34 receiver functions. In both cases the panels on the left show the individual receiver functions before stacking, while the top panels show the receiver function after stacking. The panels on the right display the back-azimuth corresponding to each receiver function. As can be seen, the results clearly reveal a Moho converted Ps wave at 4 s.

structure beneath the WLGF. Figure 7 shows a vertical cross-section along the profile A-A' (see Figure 2).

4 Results

Figure 6 maps the Vp/Vs ratio and the Moho depth, including their associated uncertainties, in the WLGF. The results indicate that the Moho is wavy, with an average depth of approximately 32 km; its depth reaches 33 km in the northwest and its shallower depth is around 31 km near the Sanguliu pluton in the southeast of the mineralized area (Figure 6B). The WSP array is located in close proximity to the NCISP-6 broadband array that was deployed to northeast China in 2007–2008. Previous studies based on this array estimated that the Moho depth in the explored area fluctuates between 30 and 35 km (Zheng et al., 2015; Dong et al., 2022), which is consistent with our results. Due to the small size of the study area and the absence of significant sedimentary zones within the mineralized zone, the Moho depth variation is gradual, with a gradient of less than 2 km. The Moho undulations beneath the WLGF show a depth decrease from northwest to southeast, approximately delineated by the gold deposits and mineralization points in Wulong.

The Vp/Vs ratio ranges from 1.74 to 1.82 in the WLGF (Figure 6A), aligning with the average of 1.76 obtained from previous research that also explored the region using receiver functions (Li and Chen, 2019). There are significant differences in the Vp/Vs ratio in the WLGF, but its variation pattern correlates with the fault distribution in the goldfield, particularly at the central location (near the Wulong gold deposit). Here, the Vp/Vs ratio is higher, around 1.8, compared to its value at the eastern and western ends. Figure 6 shows an inverse relationship between the Vp/Vs ratio and crustal thickness, particularly near the Wulong gold deposit, where a higher Vp/Vs ratio coincides with a thinner crust.

Figure 7 shows the image of the crust obtained after stacking CCP along the reference profile A-A' (see Figure 2), in which some clear interfaces and also the Moho can be seen. The CCP results indicate a well-defined low-velocity interface located 10 km beneath the WLGF, and a high-velocity interface at 15–20 km depth (Figure 7). The depth of the high-velocity interface on the eastern side of the profile is greater than that on the western side, with the presence of faults in the Sanguliu pluton. The findings corroborate the existence of a persistent low-velocity layer (between 10 and 20 km deep) throughout the WLGF, consistent with previous research. For example, Zheng et al. (2015) used receiver functions to identify velocity inversions within the crust in the eastern Liaoning region, and found a significant decrease in crustal velocity around a depth of 10 km. Similarly, Zhan et al. (2020) used ambient seismic noise tomography and identified a widespread low-velocity zone within the crust in northeastern China at approximately 10–20 km depth. The higher resolution achieved with our dense seismic array

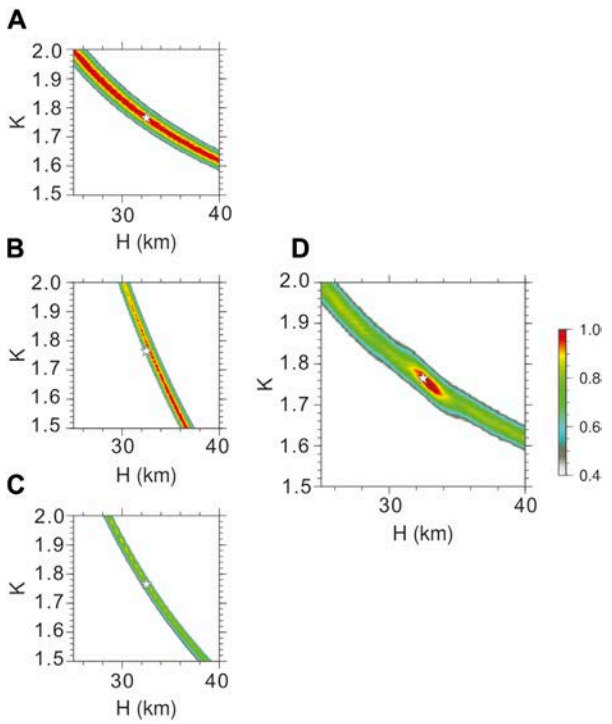

FIGURE 5
H-κ stacking results for station WL105. Panels **(A, B)** and **(C)** show the scanning results for the Ps, PpPs and PpSs+PsPs phases, respectively. Panel **(D)** on the right shows the variance obtained from the stacked amplitudes derived from the preceding three phases and utilizing Equation 1. The white star in the center of the diagram indicates the solution adopted for *H* and the Vp/Vs ratio.

allowed us to obtain more detailed features of this low-velocity layer based on CCP results.

5 Discussion

5.1 Crustal structure

The results obtained reveal an inverse relationship between the variation in the crustal thickness and the Vp/Vs ratio that is valid for the entire WLGF. The average Vp/Vs ratio for the crust is 1.76 and the Moho depth is about 32 km (Figure 6).

A correlation can be observed between the distribution of faults in the explored area and differences in the Vp/Vs ratio, which in turn are associated with the ore-containing geological structures, so that the highest values of Vp/Vs are found near the Wulong gold deposit where faults are more developed. Previous research has demonstrated that these faults are essential conduits for magmatic-hydrothermal fluid flow and that rocks near these faults (particularly near the Wulong gold deposit) have undergone intense alteration involving changes in the physical properties of the rock material in the WLGF (Zheng et al., 2022). These changes in rock properties are responsible for the differences in the crustal Vp/Vs ratio, so the high Vp/Vs ratio values observed in the Wulong gold deposit (Figure 6B) indicate the involvement of mantle-derived materials in the mineralization process. On the whole, the sulfur isotope composition of the WLGF, similar to that of the mantle (δ^{34} S: −0.9‰–3.3‰, Δ^{33} S: −0.1‰–0.2‰), rules out the contribution of Precambrian sediments and indicates the predominant contribution of mantle-derived magmatic rocks (Wei et al., 2021). The involvement of fluids from both the mantle and the Earth's crust in the mineralization process in the WLGF has also been supported by the analysis of He-Ar isotopes in fluid inclusions in pyrite samples (Liu et al., 2019). Mantle material most likely ascended to the crust through the deep Yalu River fault (Figure 2), located east of the WLGF (Zhang et al., 2018).

Given that the WLGF extends over a small area and having used a uniform one-dimensional velocity model for the entire mineralized region in the course of the H-κ scanning process, the undulations of the Moho discontinuity at this scale are almost negligible, as expected. Despite this, it can be seen that the Moho depth exhibits slight variation that appears to correlate with the spatial distribution of local faults. Based on prior geological and geophysical data, we conclude that the internal faults in the WLGF are not a sufficient cause to produce a segmented Moho (Zhang et al., 2019). Considering the correlation between the Vp/Vs ratio and Moho depth (Figure 6), we infer that the main cause of the small changes observed in Moho depth are the differences in the properties of the crustal material in the WLGF. Such differences are associated with the distribution of faults in the goldfield, which explains the correlation between changes in Moho depth and the presence of faults. The results also demonstrate the existence of relatively thin crust in the Liaodong Peninsula (Figure 7), which fits into the geodynamic framework of lithospheric thinning and tectonic extension resulting from the Mesozoic subduction of the ancient Pacific plate (Zhu et al., 2015).

5.2 Low- and high-velocity layers and mineralization process

The image of the Earth's crust in the WLGF obtained using receiver functions provides two notable features: a low-velocity interface at a depth of about 10 km and another high-velocity intracrustal interface at about 18 km depth (Figure 7). This image reveals a low-velocity layer located in the middle crust at a depth range of 10–18 km. Zhan et al. (2020) already indicated the widespread presence of this low-velocity layer in the northeastern crust of China. Considering that the depth range of the brittle-ductile transition zone in continental crust is approximately 13–18 km (England and McKenzie, 1982; Marone and Scholz, 1988; Kohlstedt et al., 1995; Mehl et al., 2005; Burov and Watts, 2006; Zhao et al., 2019), we infer that the aforementioned low-velocity layer represents a brittle-ductile transition zone widely present in the study goldfield. Based on the statistical analysis of 31,282 shallow-focus earthquakes from 1970 to 2000, Zhang et al. (2002) found that the average focal depth in Northeast China is 11 km, and the lower bound of the focal depth (D90) is 19 km. This closely matches our proposed brittle-ductile transition zone range of 10–18 km, strongly supporting our conclusions. The observed pronounced amplitudes on the top boundary of the low-velocity layer in the middle crust suggest a sharp velocity discontinuity, likely representing a brittle

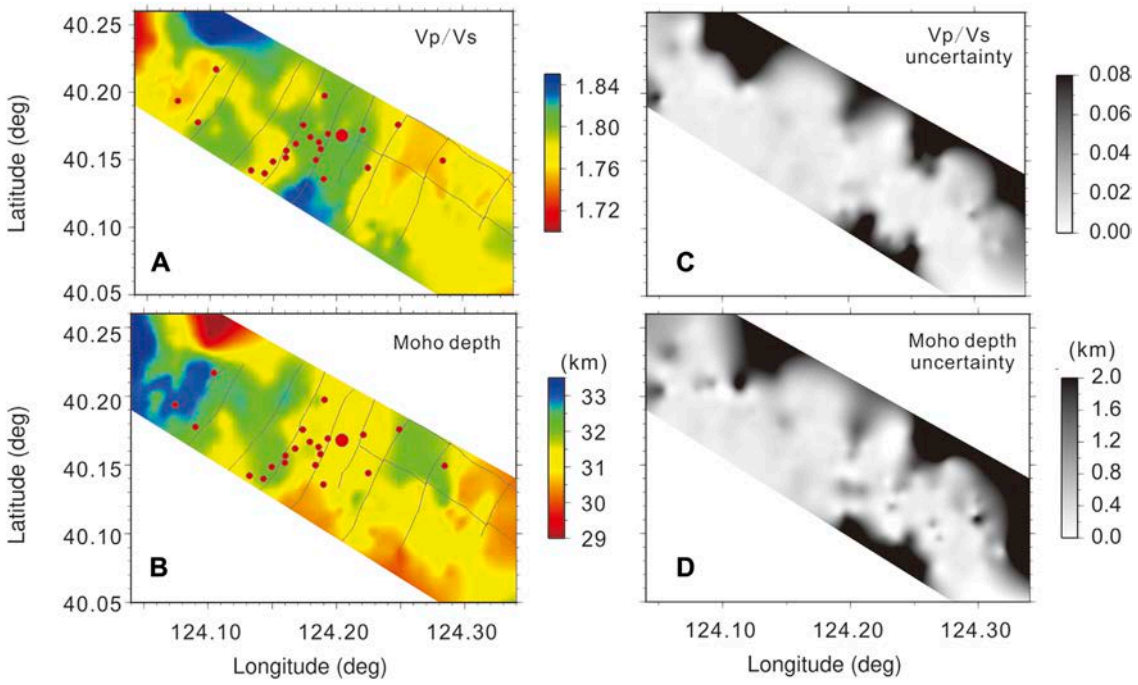

FIGURE 6
Upper plots **(A, C)**: Variations of the Vp/Vs ratio with associated uncertainties in the WLGF. Lower plots **(B, D)**: Moho depth fluctuations with associated uncertainties (respective scales on the right of each plot). Red circles indicate gold deposits or mines in Wulong.

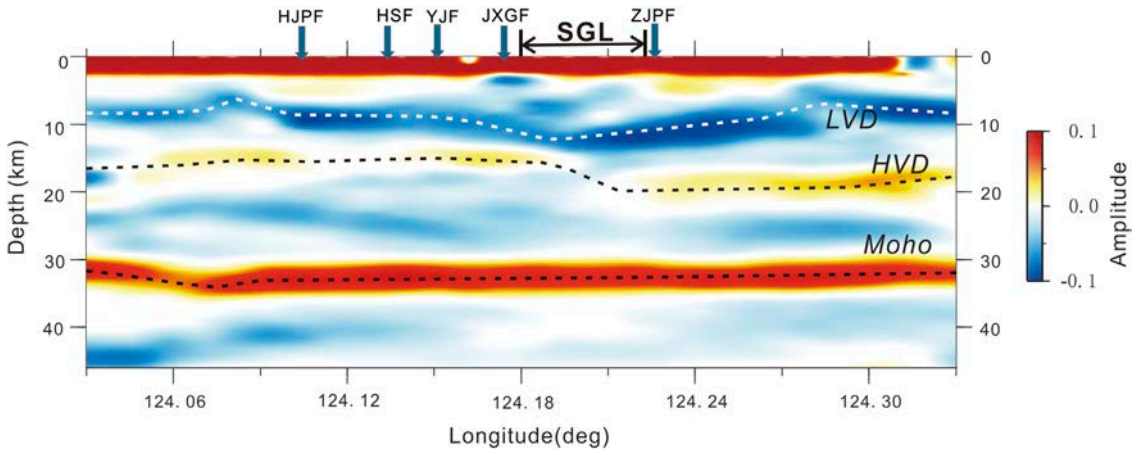

FIGURE 7
The result obtained after stacking CCP images along the profile A-A' (see Figure 2). Acronyms: HJPF, Hanjiapu Fault; HSF, Hongshi Fault; YJF, Yangjia Fault; JXGF, Jixingou Fault; ZJPF, Zhengjiapu Fault. SGL means Sanguliu Pluton. LVD means low-velocity discontinuity and HVD high-velocity discontinuity.

interface between the upper and middle crusts. In change, the bottom limit of this low-velocity layer shows weaker amplitudes and a smooth velocity gradient, possibly formed by a series of interfaces within the ductile transition zone between the middle and lower crust.

On the other hand, CCP stacking images reveal a notable structural change related to mineralization in the WLGF and associated with the Sanguliu pluton (Figure 7): the low-velocity layer seems to be fragmented and extended towards the surface. Two scenarios can explain these results: either there are major faults that cross the detected crustal low-velocity layer, or there are channels for the upwelling of magmatic-hydrothermal fluids. Previous results indicate that the faults in the WLGF are relatively shallow and do not extend to the middle crust (Zheng et al., 2022). Therefore, we conclude that there may be pathways for mineral-forming fluids to ascend in the upper crust beneath the Sanguliu pluton, causing

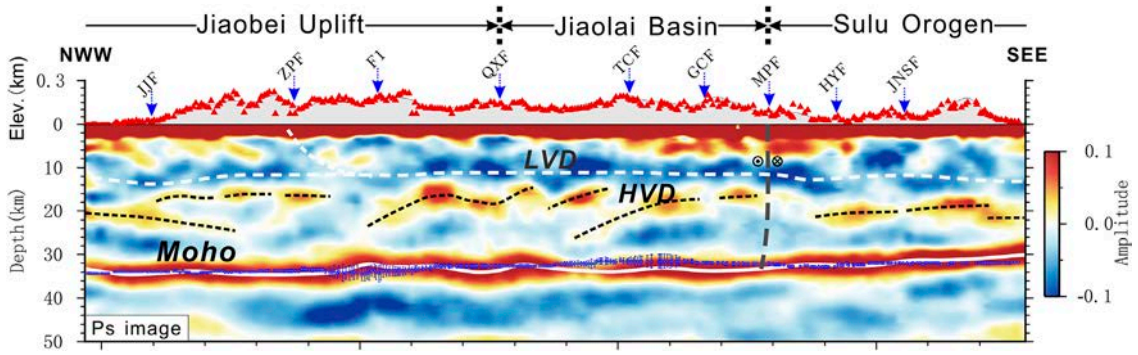

FIGURE 8
Receiver function imaging results for the Jiaodong Peninsula (Yu et al., 2020c). Acronyms: NCC, North China Craton; SCB, South China Craton; JJF, ZPF, F1, QXF, TCF, GCF, MPF, HYF, JNSF represent different faults in the Jiaodong Peninsula; LVD means low-velocity discontinuity and HVD high-velocity discontinuity.

mineralization processes to contribute to the geological complexity of this area.

We think that both crustal and mantle-derived materials have contributed to the mineralization process in the WLGF. The Yalu River fault east of the WLGF serves as a conduit for the upward migration of deep-seated mantle-derived hydrothermal fluids (Yu et al., 2018). These fluids, originating in the deep mantle, move upwards through ore-controlling structures to the middle crust. They subsequently migrate and accumulate in the WLGF along brittle-ductile shear zones (low velocity zones), and then continue to ascend along hydrothermal upwelling channels. Ultimately, they accumulate and precipitate as ore along secondary faults (NNE- and NW- trending faults) present in the goldfield.

5.3 Gold ore formation on the Liaodong Peninsula

Previous studies have suggested that the Liaodong and Jiaodong Peninsulas share similar tectonic backgrounds and metallogenic conditions (Zhang et al., 2003; Zhu et al., 2015; Yu et al., 2020c; Yu et al., 2020d; Wang et al., 2023). As we have already noted, the crustal structure in the WLGF is consistent with that reported for the Jiaodong Peninsula using receiver functions with a dense array and ambient noise images (Figure 8), where the average crustal thickness is 33 km and the average Vp/Vs ratio is 1.76 (Yu et al., 2020c). The similarity in crustal features of the Jiaodong and Liaodong Peninsulas indicates that our results may be valid for analyzing the deep subsurface seismic structure of these two areas. Furthermore, the most prominent feature of the results obtained here, the low-velocity layer, is also observed on the Jiaodong Peninsula. The low-velocity layer in the middle crust at Liaodong extends over a thickness range of 10–18 km, while at Jiaodong the top interface is about 12 km deep and the bottom interface is 16–20 km deep. This low-velocity layer may be a broad brittle-ductile transition zone, affected by mineralization-related hydrothermal alteration. On both peninsulas this low-velocity layer is discontinuous beneath the main mining areas, and faults crossing it may also be related to mineralization. It means the presence of magma conduits or faults for the upward migration of ore-forming fluids, thus providing the necessary conditions for the concentration and precipitation of minerals. Hence, the detection of such a low-velocity discontinuous layer in the middle crust may be instructive for gold exploration in the eastern NCC.

The similarity in the deep structure and mineralization history of the two peninsulas encourages us to think that the Liaodong area has mineralization potential. Nevertheless, by comparing the control structures, hidden plutons, ore-hosting rocks and other mineral-forming factors on both peninsulas, it is evident that the Liaodong goldfield is generally at a lower level of mineralization. Low-temperature thermochronological studies indicate that the evolution at Jiaodong and Liaodong was similar during the Cretaceous. However, during this time significant differences in uplift patterns emerged and Jiaodong experienced greater exhumation (Wang et al., 2018; Wang et al., 2022). This supports the idea that the Liaodong Peninsula is still at a lower level in terms of mineralization. The difference in mineralization stage with respect to the Jiaodong Peninsula can be attributed to the lateral heterogeneity resulting from the subduction of the Mesozoic Pacific Plate, together with regional extension and uplift (Meng et al., 2022).

In summary, the Jiaodong and Liaodong Peninsulas share a similar overall geological background, including a characteristic low-velocity layer located in the middle crust. Although Liaodong has an upper crust that is at a not so advanced stage of mineralization as Jiaodong, this does not reduce its promising ore formation prospects, which should be an incentive for future prospecting work.

6 Conclusion

In this paper, we have used receiver functions to obtain a detailed image of the crust in the WLGF, thus facilitating the explanation of the process associated with gold mineralization in the Liaodong Peninsula. The most remarkable results regarding the explored region are the following:

1) The crust in the WLGF is characterized by an average thickness of approximately 32 km and a Vp/Vs ratio of 1.76, although

it shows some lateral heterogeneity. In particular, the highest values of the Vp/Vs ratio (~1.8) are found near the Wulong gold deposit and suggest a possible involvement of mantle material in the mineralization process. Both the sulfur isotopic composition of the WLGF, which is similar to that of the mantle, and the analysis of He-Ar isotopes in fluid inclusions support the contribution of mantle-derived magmatic rocks.

2) Below the WLGF, a low-velocity layer is detected at a depth of 10–18 km, which can be considered as a widespread brittle-ductile transition zone in the continental crust. This low-velocity layer seems to be fragmented below the Sanguliu pluton and this gives us cause to think about pathways for the ascent of ore-forming fluids in the upper crust causing mineralization.
3) Considering that the Liaodong and Jiaodong Peninsulas share similar tectonic environments and metallogenic conditions, even a characteristic low-velocity layer located in the middle crust, and even admitting that the Liaodong goldfield is generally at a lower level of mineralization, there are still a wide scope for future prospecting work focused on ore-containing formations.

Data availability statement

The raw data supporting the conclusions of this article will be made available by the authors, without undue reservation.

Author contributions

FZ: Funding acquisition, Visualization, Writing–original draft, Writing–review and editing. TX: Methodology, Resources, Supervision, Writing–review and editing. YA: Investigation, Project administration, Writing–review and editing. YG: Formal Analysis, Funding acquisition, Resources, Writing–review and editing. QZ: Conceptualization, Data curation, Methodology, Writing–original draft. LM: Methodology, Supervision, Writing–original draft. WD: Investigation, Visualization, Writing–review and editing. JB: Formal Analysis, Writing–review and editing.

Funding

The author(s) declare that financial support was received for the research, authorship, and/or publication of this article. This research was funded by grants from the aforementioned institutions (42104102, 42130807, 42374060, 2016YFC0600101, MBP00403D) and Key Laboratory of Target Cognition and Application Technology (TCAT), Aerospace Information Research Institute, Chinese Academy of Sciences.

Acknowledgments

We are grateful to the following institutions for their assistance and help during the data acquisition time period: Liaohe Geophysical Exploration Company, Seismic Array Laboratory, Institute of Geology and Geophysics, Chinese Academy of Sciences, Southern University of Science and Technology, and Guilin University of Technology. We would like to thank Profs. Tianyu Zheng, Jinhui Yang, Xiaobo Tian, Yingjie Yang and Yongqian Zhang, Zhenbo Wu, Guiping Yu, Lu Zhang for their constructive comments that allowed us to improve the quality of the early manuscript. We would like to thank the National Natural Science Foundation of China (42104102, 42130807, 42374060), the Chinese National Key Research and Development Program (2016YFC0600101) and the independent research project of Key Laboratory of Target Cognition and Application Technology (TCAT, MBP00403D).

Conflict of interest

The authors declare that the research was conducted in the absence of any commercial or financial relationships that could be construed as a potential conflict of interest.

Publisher's note

References

Burov, E. B., and Watts, A. B. (2006). The long-term strength of continental lithosphere:"jelly sandwich" or "crème brûlée". *GSA today* 16, 4–10. doi:10.1130/1052-5173(2006)016<4:tltsoc>2.0.co;2

Deng, J., Yang, L. Q., Groves, D. I., Zhang, L., Qiu, K. F., and Wang, Q. F. (2020). An integrated mineral system model for the gold deposits of the giant Jiaodong province, eastern China. *Earth-Science Rev.* 208, 103274. doi:10.1016/j.earscirev.2020.103274

Di, Q. Y., Xue, G. Q., Lei, D., Zeng, Q. D., Fu, C. M., and An, Z. G. (2021). Summary of technology for a comprehensive geophysical exploration of gold mine in North China Craton. *Sci. China-Earth Sci.* 64, 1524–1536. doi:10.1007/s11430-020-9818-2

Dong, W. Y., Xu, T., Ai, Y. S., Fan, E. B., Li, L., and Hou, J. (2022). The boundary between the North China craton and the central asian orogenic belt in NE China: seismic evidence from receiver function imaging. *J. Asian Earth Sci.* 237, 105360. doi:10.1016/j.jseaes.2022.105360

England, P., and McKenzie, D. (1982). A thin viscous sheet model for continental deformation. *Geophys. J. Int.* 70, 295–321. doi:10.1111/j.1365-246x.1982.tb04969.x

Gu, Y. C., Zhao, Y., Yang, Z. Z., Zhang, P., Yang, F. C., Ju, N., et al. (2020). Zircon U-Pb ages, elements geochemistry and Sr-nd-Pb-Hf isotopic characteristics of the Wulong remelting granite intrusive rocks in Liaodong Peninsula and Geological significance. *Earth Sci.* 445, 1–34. doi:10.3799/dqkx.2020.220

Jiang, X., Yang, H., Yang, W., and Wang, W. (2020). Crustal structure in the binchuan basin of yunnan constrained from receiver functions on a 2-d seismic dense array. *Earthq. Sci.* 33, 264–272. doi:10.29382/eqs-2020-0264-01

Kohlstedt, D. L., Evans, B., and Mackwell, S. J. (1995). Strength of the lithosphere: constraints imposed by laboratory experiments. *J. Geophys. Res. Solid Earth* 100, 17587–17602. doi:10.1029/95jb01460

Li, T. J., and Chen, Q. F. (2019). Crustal structure of different tectonic units in southeastern part of Northeast China using receiver functions. *Chin. J. Geophys.* 62, 2899–2917. doi:10.6038/cjg2019M0379

Ligorría, J. P., and Ammon, C. J. (1999). Iterative deconvolution and receiver-function estimation. *Bull. Seismol. Soc. Am.* 89, 1395–1400. doi:10.1785/bssa0890051395

Liu, G., Persaud, P., and Clayton, R. W. (2018). Structure of the northern los angeles basins revealed in teleseismic receiver functions from short-term nodal seismic arrays. *Seismol. Res. Lett.* 89 (5), 1680–1689. doi:10.1785/0220180071

Liu, J., Zhang, L. J., Wang, S. L., Li, T. G., Yang, Y., Liu, F. X., et al. (2019). Formation of the Wulong gold deposit, Liaodong gold Province, NE China: constraints from zircon U–Pb age, sericite Ar–Ar age, and H–O–S–He isotopes. *Ore Geol. Rev.* 109, 130–143. doi:10.1016/j.oregeorev.2019.04.013

Lythgoe, K. H., Ong, S, Qing, M., and Wei, S. (2020). Large-scale crustal structure beneath singapore using receiver functions from a dense urban nodal array. *Geophys. Res. Lett.* 47 (7), e2020GL087233. doi:10.1029/2020gl087233

Ma, L. X., Xu, T., Ai, Y. S., Yang, J. H., Yang, Y. J., Fan, E. B., et al. (2022). Hot lithosphere beneath the northeastern North China Craton detected by ambient noise tomography. *Tectonophysics* 839, 229551. doi:10.1016/j.tecto.2022.229551

Marone, C., and Scholz, C. (1988). The depth of seismic faulting and the upper transition from stable to unstable slip regimes. *Geophys. Res. Lett.* 15, 621–624. doi:10.1029/gl015i006p00621

Mehl, C., Jolivet, L., and Lacombe, O. (2005). From ductile to brittle: evolution and localization of deformation below a crustal detachment (Tinos, Cyclades, Greece). *Tectonics* 24, 1–23. doi:10.1029/2004tc001767

Meng, F. C., Ai, Y. S., Xu, T., Chen, L., Wang, X., and Li, L. (2021). Lithospheric structure beneath the boundary region of north China craton and xing Meng orogenic belt from S-receiver function analysis. *Tectonophysics* 818, 229067. doi:10.1016/j.tecto.2021.229067

Meng, Q. R., Zhou, Z. H., Zhu, R. X., Xu, Y. G., and Guo, Z. T. (2022). Cretaceous basin evolution in northeast Asia: tectonic responses to the paleo-Pacific plate subduction. *Natl. Sci. Rev.* 9, nwab088. doi:10.1093/nsr/nwab088

Santosh, M., Tsunogae, T., Li, J. H., and Liu, S. J. (2007). Discovery of sapphirine-bearing Mg–Al granulites in the North China Craton: implications for Paleoproterozoic ultrahigh temperature metamorphism. *Gondwana Res.* 11, 263–285. doi:10.1016/j.gr.2006.10.009

Song, M. C. (2015). The main achievements and key theory and methods of deep-seated prospecting in the Jiaodong gold concentration area, Shandong Province. *Geol. Bull. China* 34, 1758–1771. doi:10.3969/j.issn.1671-2552.2015.09.017

Wang, Y. Z., Wang, F., Wu, L., Shi, W. B., and Yang, L. K. (2018). (U-Th)/He thermochronology of metallic ore deposits in the Liaodong Peninsula: implications for orefield evolution in northeast China. *Ore Geol. Rev.* 92, 348–365. doi:10.1016/j.oregeorev.2017.11.025

Wang, Y. Z., Wang, F., Wu, L., Zhang, Z. Y., Shi, W. B., and Yang, L. K. (2022). Differential post-mineralization thermal evolution of the Jiaodong and Liaodong Areas, Eastern China: an indicator of regional tectonic activity. *Gondwana Res.* 103, 502–521. doi:10.1016/j.gr.2021.11.006

Wang, Z. C., Wang, X., Zong, K. Q., Cheng, H., Wang Christina, Y., Li, J. W., et al. (2023). The secular crust-mantle evolution of the North China Craton and the formation of giant Jiaodong gold deposits. *Bull. Mineralogy Petrology Geochem.* 42, 1231–1247. doi:10.19658/j.issn.1007-2802.2023.42.097

Wang, Z. Q., Hu, H. Z. F., Chen, B., Duan, X. X., Zhou, T. F., and Jiang, X. (2020). The petrogenesis of the Early Cretaceous Sanguliu pluton in the Liaodong Peninsula, NE China: constrained from the trace-element modelling and Sr-Nd isotopes. *Acta Petrol. Sin.* 36, 3683–3704. doi:10.18654/1000-0569/2020.12.08

Wei, B., Wang, C. Y., Wang, Z. C., Cheng, H., Xia, X., and Tan, W. (2021). Mantle-derived gold scavenged by bismuth-(tellurium)-rich melts: evidence from the mesozoic wulong gold deposit in the north China craton. *Ore Geol. Rev.* 131, 104047. doi:10.1016/j.oregeorev.2021.104047

Wei, J. H., Liu, C. Q., Zhao, Y. X., and Li, Z. D. (2001). Time span of the major ore-forming stages of the Wulong gold deposit. *Liaoning, Geol. Rev.* 47, 433–437. doi:10.16509/j.georeview.2001.04.021

Wei, J. H., Qiu, X. P., Guo, D. Z., and Tan, W. J. (2004). Geochemistry of ore fluids and Rb-Sr isotopic dating for the wulong gold deposit in liaoning, China. *Acta Geol. Sinica-English Ed.* 78, 1267–1274. doi:10.1111/j.1755-6724.2004.tb00784.x

Wei, Y., Tian, X., Duan, Y., and Tian, X. (2018). Imaging the topography of crust–mantle boundary from a high-density seismic array beneath the middle-lower yangtze river, eastern China. *Seismol. Res. Lett.* 89 (5), 1690–1697. doi:10.1785/0220180045

Wu, F. Y., Yang, J. H., and Liu, X. M. (2005). Geochronological framework of the mesozoic granitic magmatism in the Liaodong peninsula, northeast China. *Geol. J. China Univ.* 11, 305–317. doi:10.3969/j.issn.1006-7493.2005.03.003

Xie, T. T., Xu, T., Ai, Y. S., Zeng, Q. D., Zhang, W., and Zheng, F. (2021). Imaging the shallow crustal velocity structure of the Qingchengzi ore field on the Liaodong Peninsula, China, with a short-period dense array using ambient noise tomography. *Tectonophysics* 813, 228913. doi:10.1016/j.tecto.2021.228913

Yu, B., Zeng, Q. D., Frimmel, H. E., Qiu, H. C., Li, Q. L., Yang, J. H., et al. (2020a). The 127 Ma gold mineralization in the Wulong deposit, Liaodong Peninsula, China: constraints from molybdenite Re-Os, monazite U-Th-Pb, and zircon U-Pb geochronology. *Ore Geol. Rev.* 121, 103542. doi:10.1016/j.oregeorev.2020.103542

Yu, B., Zeng, Q. D., Frimmel, H. E., Wang, Y., Guo, W., Sun, G., et al. (2018). Genesis of the wulong gold deposit, northeastern north China craton: constraints from fluid inclusions, hos-pb isotopes, and pyrite trace element concentrations. *Ore Geol. Rev.* 102, 313–337. doi:10.1016/j.oregeorev.2018.09.016

Yu, B., Zeng, Q. D., Xia, F., Qiu, H. C., Li, J. P., Xie, L. Q., et al. (2020b). Structural superimposed halo of the Wulong gold deposit in Liaoning Province. *Geol. Explor.* 56, 898–914. doi:10.12134/j.dzykt.2020.05.002

Yu, G. P., Xu, T., Ai, Y. S., Chen, L., and Yang, J. H. (2020c). Significance of crustal extension and magmatism to gold deposits beneath Jiaodong Peninsula, eastern North China Craton: seismic evidence from receiver function imaging with a dense array. *Tectonophysics* 789, 228532. doi:10.1016/j.tecto.2020.228532

Yu, G. P., Xu, T., Liu, J. T., and Ai, Y. S. (2020d). Late Mesozoic extensional structures and gold mineralization in Jiaodong Peninsula, eastern North China Craton: an inspiration from ambient noise tomography on data from a dense seismic array. *Chin. J. Geophys.* 63, 1878–1893.

Zeng, Q. D., Chen, R. Y., Yang, J. H., Sun, G. T., Yu, B., Wang, Y. B., et al. (2019). The metallogenic characteristics and exploring ore potential of the gold deposits in eastern Liaoning Province. *Acta Petrol. Sin.* 35, 1939–1963. doi:10.18654/1000-0569/2019.07.01

Zhan, W., Pan, L., and Chen, X. F. (2020). A widespread mid-crustal low-velocity layer beneath Northeast China revealed by the multimodal inversion of Rayleigh waves from ambient seismic noise. *J. Asian Earth Sci.* 196, 104372. doi:10.1016/j.jseaes.2020.104372

Zhang, B., Lei, J., Yuan, X., Zhang, G., He, J., and Xu, Q. (2020). Detailed moho variations under northeast China inferred from receiver function analyses and their tectonic implications. *Phys. Earth Planet. Interiors* 300, 106448. doi:10.1016/j.pepi.2020.106448

Zhang, G. M., Wang, S. Y., Li, L., Zhang, X. D., and Ma, H. S. (2002). Focal depth of earthquakes in the Chinese mainland and its tectonic significance. *Chin. Sci. Bull.* 47, 663–668. doi:10.1360/csb2002-47-9-663

Zhang, S., Zhu, G., Liu, C., Li, Y. J., Su, N., Xiao, S. Y., et al. (2018). Strike-slip motion within the Yalu River Fault Zone, NE Asia: the development of a shear continental margin. *Tectonics* 37, 1771–1796. doi:10.1029/2018tc004968

Zhang, Y. Q., Ma, Y. S., Yang, N., Shi, W., and Dong, S. W. (2003). Cenozoic extensional stress evolution in North China. *J. Geodyn.* 36, 591–613. doi:10.1016/j.jog.2003.08.001

Zhang, Z., Deng, Y., Yao, J., Zong, J., and Chen, H. (2021). An array based seismic image on the dahutang deposit, south China: insight into the mineralization. *Phys. Earth Planet. Interiors* 310, 106617. doi:10.1016/j.pepi.2020.106617

Zhang, Z. Q., Wang, G. W., Carranza, E. J. M., Zhang, J. J., Tao, G. S., Zeng, Q. D., et al. (2019). Metallogenic model of the Wulong gold district, China, and associated assessment of exploration criteria based on multi-scale geoscience datasets. *Ore Geol. Rev.* 114, 103138. doi:10.1016/j.oregeorev.2019.103138

Zhao, T., Xie, C. L., and Xiang, B. W. (2019). Deformation process and mechanism of the brittle-ductile transition zone: evidence from the southern segment of the Tan-Lu fault zone. *Geotect. Metallogenia* 43, 17–32. doi:10.16539/j.ddgzyckx.2019.01.002

Zheng, F., Xu, T., Ai, Y. S., Yang, Y. J., Zeng, Q. D., Yu, B., et al. (2022). Metallogenic potential of the Wulong goldfield, Liaodong Peninsula, China revealed by high-resolution ambient noise tomography. *Ore Geol. Rev.* 142, 104704. doi:10.1016/j.oregeorev.2022.104704

Zheng, T. Y., He, Y. M., Yang, J. H., and Zhao, L. (2015). Seismological constraints on the crustal structures generated by continental rejuvenation in northeastern China. *Sci. Rep.* 5, 14995. doi:10.1038/srep14995

Zhu, L. P., and Kanamori, H. (2000). Moho depth variation in southern California from teleseismic receiver functions. *J. Geophys. Res. Solid Earth* 105, 2969–2980. doi:10.1029/1999jb900322

Zhu, R. X., Fan, H. R., Li, J. W., Meng, Q. R., Li, S. R., and Zeng, Q. D. (2015). Decratonic gold deposits. *Sci. China Earth Sci.* 58, 1523–1537. doi:10.1007/s11430-015-5139-x